A partition of unity FEM for time-dependent diffusion problems using multiple enrichment functions

A partition of unity finite element method for time dependent diffusion problems using multiple enrichment functions

M. Shadi Mohamed[*] Mohammed Seaid[*] Jon Trevelyan[*] Omar Laghrouche[†]

Abstract

An enriched partition of unity finite element method is developed to solve time dependent diffusion problems. In the present formulation, multiple exponential functions describing the spatial and temporal diffusion decay are embedded in the finite element approximation space. The resulting enrichment is in the form of a local asymptotic expansion. Unlike previous works in this area where the enrichment must be updated at each time step, here the temporal decay in the solution are embedded in the asymptotic expansion. Thus the system matrix which is evaluated at the first time step may be decomposed and retained for every next time step by just updating the right hand side of the linear system of equations. The advantage is a significant saving in the computational effort where previously the linear system must be reevaluated and resolved at every time step. In comparison with the traditional finite element analysis with p-version refinements, the present approach is much simpler, more efficient, and yields more accurate solutions for a prescribed number of degrees of freedom. Numerical results are presented for a transient diffusion equation with known analytical solution. The performance of the method is analyzed on two applications: the transient heat equation with a single source and with multiple sources. The aim of such a method compared to the classical finite element method is to solve time dependent diffusion applications efficiently and with an appropriate level of accuracy.

Keywords. Finite element method; partition of unity method; time dependent equations; diffusion problems

1 Introduction

In recent decades, finite element methods have offered a remarkable level of accuracy and robustness required for solving complex potential problems governed by steady state differential equations (PDEs) of elliptic type. However, engineering applications often involve time dependent partial differential equations which have to be solved on complex geometries, thus suggesting the use of discretization of both space and time variables. In practice, the focus is on unstructured meshes where a nontrivial reconstruction scheme is required to have a high order spatial accuracy. Most classical finite element methods for unstructured grids proposed to date employ linear or quadratic elements. However, solving time dependent diffusion equations using finite element methods is still a considerable task in the case of unstructured meshes; particularly when these equations have to be solved in conjunction with PDEs of hyperbolic type [1]. It is well known that the solutions of these coupled problems present steep fronts, boundary layers, and even shock discontinuities, which need to be resolved accurately in applications and often cause severe numerical difficulties [2, 3].

Time dependent diffusion equations are used in many physical and engineering applications, for example, to describe cooling down of molten glass or heat transfer in enclosures. In glass manufacturing, a hot melt of glass is cooled down to room temperature. This annealing must be monitored carefully to avoid excessive temperature differences, which may affect the quality of the

[*]School of Engineering and Computing Sciences, Durham University, South Road, Durham DH1 3LE, UK
[†]School of the Built Environment, Heriot-Watt University, Edinburgh EH14 4AS, UK

product or even lead to cracking [4, 5]. To control the annealing process, the transient diffusion equations may be used to predict accurately the temperature evolution in the glass. In addition, time dependent diffusion equations are also used to model several problems in thermal radiation heat transfer [6] and optical tomography [7] among others. In general, thermal radiation has to be modeled by equations that involve the direction and frequency dependent thermal radiation field due to the energy transport by photons. However, using asymptotic expansions, the full radiative transfer equation can be replaced by a class of non-stationary diffusion equations equipped with Robin boundary conditions that depend on space and time but not direction. Such practical time dependent diffusion problems are not trivial to simulate since the geometry can be complex and internal source/sink terms may produce steep gradient (solution peaks) propagating along the computational domain. It is well known that unstructured grids can be highly advantageous based on their ability to provide local mesh refinement near important diffusion features and structures. As a consequence, the ability to provide local mesh refinement where it is needed leads to improved accuracy for a given computational cost as compared to methods that use structured meshes.

One solution that has emerged in the literature is the idea of injecting enrichment functions into the finite element approximation space. These techniques fall under the general heading of Partition of Unity Methods (PUM) [8], so called because the partition of unity property of traditional interpolating shape functions allows enrichment functions to be undistorted through their combination with these shape functions. The enrichment functions may be of different characters. Ideally they comprise either the asymptotic solution space or sets of functions known to be complete for the PDE at hand. An example of taking enrichment functions from asymptotic fields is found in the eXtended Finite Element Method (XFEM), where a basis for expressing the displacement found locally around crack tips is found from classical expansions found in fracture mechanics [9]. There is also a large body of literature in the meshless methods [10] and boundary element [11] communities using similarly derived enrichment functions for cracks. An example of taking a set of enrichment functions known to be complete for the PDE is in expressing wave potential as a linear combination of a set of plane waves. Instances of this approach are available in the literature for the Partition of Unity Finite Element Method (PUFEM) [12, 13, 14], boundary element method [15, 16], ultraweak formulations [17, 18, 19] and discontinuous Galerkin methods [20, 21, 22] for the solution of Helmholtz (e.g. acoustic) and elastic wave problems. The PUM idea has also been presented in the context of the Generalized Finite Element Method (GFEM) [23, 24, 25]. Formulations are emerging in which the enrichment functions themselves are determined adaptively [26, 27].

A further classification of enrichment includes the use of functions that *approximate* the solution in some way. While this may be less rigorous mathematically, these methods are attractive for practical use in cases in which no suitable analytical solution space is available to form the enrichment basis. We give evidence in this paper that such approximate enrichment functions allow for improved accuracy for a prescribed number of degrees of freedom. All of these PUM methods are easy to formulate and implementation in existing codes may be carried out without large scale restructuring of the code. Some care needs to be taken to avoid (or at least ameliorate) problems of ill conditioning which are reported in many PUM works. However, in spite of the potential for ill conditioned systems, these approaches have been consistently shown to reduce errors in comparison with conventional piecewise polynomial bases. Enrichment functions have recently been applied to problems involving transient thermal effects [28]. van der Meer *et al.* [29] developed a set of algorithms to study time dependent geothermal problems using enrichment functions that approximate the solution at each time step. The evolution of thermal gradients with time is considered by updating the shape functions so that they remain optimal at each time. O'Hara *et al.* [30] presented a global local GFEM formulation for transient heat transfer, in which a linear interpolative basis is augmented by an exponential function of space or space and time as well. Time dependent shape functions are used to handle the transient nature of the problem, and these are supplemented by local analysis using various techniques in regions of high thermal gradient.

In the current work, we introduce a PUFEM approach for the solution of transient diffusion

problems which uses a multiplicity of approximate enrichment functions. We use Gaussian functions of varying standard deviations to form the enrichment, and these are used in combination with a piecewise linear Lagrangian polynomial finite element discretization so that the global Gaussian surfaces are modulated locally. A notable feature of the approach is that the same (enriched) approximation space is used at each time step. The more rapidly varying enrichment functions are useful for early time steps around localized thermal sources, while other (flatter) enrichment functions become important both in the far field and more generally as a steady state is approached. In other words there is no requirement for time dependent shape functions. By doing so, the system matrix may be decomposed at the first time step and retained to be reused with just updating the right hand side of the linear system of equations at all the following time steps. This can significantly reduce the computational costs when compared to other available enrichment techniques where the full linear system must be updated and resolved repeatedly. Especially that the computational time required to building the linear system may be increased significantly by the time spent on numerical integrating complicated enrichment functions over relatively large elements. Further, the approach presented here may be generalized by locating different Gaussian functions at different centers, allowing for efficient solutions of problems with multiple sources.

This paper is organized in the following fashion. In section 2 we introduce the governing PDE for transient diffusion, the initial and boundary conditions and the transformation to the weak form. The Partition of Unity enrichment is presented in section 3, and its effectiveness is demonstrated for a range of numerical test cases in section 4. We close in section 5 with some concluding remarks.

2 Boundary value problem and weak form

Given an open bounded domain $\Omega \subset \mathbb{R}^2$ with a boundary Γ and a given time interval $[0, T]$, we are interested in this paper to study the following transient diffusion equations: find $u :]0, T[\times\Omega \longrightarrow \mathbb{R}^2$ such that

$$\frac{\partial u}{\partial t} - \lambda \nabla^2 u = f(t, \mathbf{x}), \qquad (t, \mathbf{x}) \in]0, T[\times\Omega, \tag{1}$$

where $\mathbf{x} = (x, y)^T$ denotes the spatial coordinates, t is the time variable, λ is the diffusion coefficient, and f represents the effects of internal sources/sinks. We consider an initial condition

$$u(t = 0, \mathbf{x}) = u_0(\mathbf{x}), \qquad \mathbf{x} \in \ \Omega, \tag{2}$$

where u_0 is a prescribed initial field. The above equations are to be solved subject to the boundary condition

$$\alpha u + \frac{\partial u}{\partial \mathbf{n}} = g(t, \mathbf{x}), \qquad (t, \mathbf{x}) \in]0, T[\times\Gamma, \tag{3}$$

where $\mathbf{n}$ is the outward unit normal on the boundary Γ, and g is a given boundary function.

To integrate the equations (1)-(3) we divide the time interval into N_t subintervals $[t_n, t_{n+1}]$ with duration $\Delta t = t_{n+1} - t_n$ for $n = 0, 1, \ldots, N_t$. We use the notation w^n to denote the value of a generic function w at time t_n. We may consider a θ-time stepping integration scheme, in which the semi-discrete formulation of the diffusion problem (1) is given by

$$\frac{u^{n+1} - u^n}{\Delta t} - (1 - \theta)\lambda \nabla^2 u^{n+1} - \theta \lambda \nabla^2 u^n \ = \ (1 - \theta) f^{n+1} + \theta f^n, \tag{4}$$

where the parameter θ has to be chosen depending on the time stepping scheme; by taking $\theta = 0$ the equation (4) is the first order Backward Euler scheme which is unconditionally stable for linear problems, so that the choice of Δt may be based on the accuracy to be achieved in the computed solutions. To find the solution u^{n+1} from (4) one has to solve, at each time level, a linear system of algebraic equations. By setting $\theta = 0$ the equation (4) becomes

$$\frac{u^{n+1} - u^n}{\Delta t} - \lambda \nabla^2 u^{n+1} = f^{n+1}. \tag{5}$$

This can be rearranged as

$$u^{n+1} - \lambda \Delta t \nabla^2 u^{n+1} = F, \tag{6}$$

where F is defined as

$$F = \Delta t f^{n+1} + u^n.$$

We may proceed as in conventional finite element formulations by multiplying equation (6) by a weighting function, W, and then integrating over Ω, yielding

$$\int_\Omega W u^{n+1} d\Omega - \int_\Omega \lambda \Delta t W \nabla^2 u^{n+1} d\Omega = \int_\Omega W F d\Omega. \tag{7}$$

Using the divergence theorem one may write

$$\int_\Omega W \nabla^2 u^{n+1} d\Omega = \int_\Gamma W \nabla u^{n+1} \cdot \mathbf{n} d\Gamma - \int_\Omega \nabla W \cdot \nabla u^{n+1} d\Omega. \tag{8}$$

Substituting (8) into (7) results in

$$\int_\Omega W u^{n+1} d\Omega - \int_\Gamma \lambda \Delta t W \nabla u^{n+1} \cdot \mathbf{n} d\Gamma + \int_\Omega \lambda \Delta t \nabla W \cdot \nabla u^{n+1} d\Omega = \int_\Omega W F d\Omega,$$

or simply

$$\int_\Omega (\lambda \Delta t \nabla W \cdot \nabla u^{n+1} + W u^{n+1}) d\Omega - \int_\Gamma \lambda \Delta t W \nabla u^{n+1} \cdot \mathbf{n} d\Gamma = \int_\Omega W F d\Omega.$$

Substituting the boundary condition in equation (3) gives us the statement of the problem to be solved in weak form, i.e. find $u \in H^1(\Omega)$ such that:

$$\int_\Omega (\lambda \Delta t \nabla W \cdot \nabla u^{n+1} + W u^{n+1}) d\Omega + \oint_\Gamma \lambda \Delta t W (\alpha u^{n+1} - g^{n+1}) d\Gamma = \int_\Omega W F d\Omega \,, \qquad \forall\, W \in H^1(\Omega), \tag{9}$$

where $H^1(\Omega)$ is the Sobolev space.

3 Partition of unity enriched finite element method

To solve the weak form (9) with the finite element method, first the domain Ω is discretized. To perform this step, we generate a quasi uniform partition $\Omega_h \subset \Omega$ of N_e elements $\mathcal{T}_j$ that satisfy the following conditions:

(i) $\Omega_h = \bigcup_{j=1}^{N_e} \mathcal{T}_j$.

(ii) If $\mathcal{T}_i$ and $\mathcal{T}_j$ are two different elements of Ω_h, then

$$\mathcal{T}_i \cap \mathcal{T}_j = \begin{cases} P_{ij}, & \text{a mesh point, or} \\ \Gamma_{ij}, & \text{a common side, or} \\ \emptyset, & \text{empty set.} \end{cases}$$

(iii) There exists a positive constant k such that for all $j \in \{1, \cdots, N_e\}$, $\frac{r_j}{h_j} > k$ $(h_j \leq h)$, where r_j is the radius of the circle inscribed in $\mathcal{T}_j$ and h_j is the largest side of $\mathcal{T}_j$.

The conforming finite element space for the solution that we use is defined as

$$V_h = \Big\{ u_h \in C^0(\Omega) : \quad u_h\big|_{\mathcal{T}_j} \in P(\mathcal{T}_j), \quad \forall\ \mathcal{T}_j \in \Omega_h \Big\}, \tag{10}$$

with

$$P(\mathcal{T}_j) = \Big\{ p(\mathbf{x}) : \quad p(\mathbf{x}) = \hat{p} \circ Y_j^{-1}(\mathbf{x}), \quad \hat{p} \in P_m(\hat{\mathcal{T}}) \Big\},$$

where $\hat{p}(\mathbf{x})$ is a polynomial of degree $\leq m$ defined on the element $\hat{\mathcal{T}}_j$ and $P_m(\hat{\mathcal{T}})$ is the set of polynomials of degree $\leq m$ defined on the element of reference $\hat{\mathcal{T}}$. Here $Y_j : \hat{\mathcal{T}} \longrightarrow \mathcal{T}_j$ is an invertible one-to-one mapping.

Next, we formulate the finite element solution to $u^n(\mathbf{x})$ as

$$u^n(\mathbf{x}) \simeq u_h^n(\mathbf{x}) = \sum_{j=1}^{N_d} C_j^n N_j(\mathbf{x}), \tag{11}$$

where N_d is the number of solution mesh points in the partition Ω_h. The functions C_j^n are the corresponding nodal values of $u_h^n(\mathbf{x})$. They are defined as $C_j^n = u_h^n(\mathbf{x}_j)$ where $\{\mathbf{x}_j\}_{j=1}^{N_d}$ are the set of solution mesh points in the partition Ω_h. In (11), $\{N_j\}_{j=1}^{N_d}$ are the set of global nodal basis functions of V_h characterized by the property $N_i(\mathbf{x}_j) = \delta_{ij}$ with δ_{ij} denoting the Kronecker symbol. We introduce $\{\mathbf{x}_1, \cdots, \mathbf{x}_M\}$ as the set of M nodal points in the element $\mathcal{T}_j$. We also define $\{\varphi_j\}_{j=1}^{M}$ as the set of element basis coefficients for $\mathcal{T}_j$ in V_h characterized by the property $\varphi_i(\mathbf{x}_j) = \delta_{ij}$. Hereafter, unless otherwise stated, the subscripts h and j are used to refer to coefficients associated with the whole mesh Ω_h and a mesh element $\mathcal{T}_j$, respectively. Note that the set $\{\varphi_j\}_{j=1}^{M}$ is a local restriction on the element $\mathcal{T}_j$ of the set of the global basis functions $\{N_j\}_{j=1}^{M}$. The approximation space is then defined as

$$\widetilde{V}_h^0 = \text{span}\left\{ N_h,\ u_h = \sum_{j=0}^{M} u_j N_j \right\}.$$

Using the partition of unity method [8] it is possible to enrich the solution space with basis functions that have better approximation properties than the conventional polynomial basis functions. To solve an elliptic partial differential equation similar to the one considered here, Li proposed a set of exponential functions [31]. Here we propose using the following sum of exponential basis functions to enrich the solution space

$$F_{enr} = \Big\{ G_1, G_2, ..., G_Q \Big\} \tag{12}$$

where

$$G_q = \frac{\exp\left(-\left(\frac{R_0}{C}\right)^q\right) - \exp\left(-\left(\frac{R_c}{C}\right)^q\right)}{1 - \exp\left(-\left(\frac{R_c}{C}\right)^q\right)}, \quad q = 1, 2, ..., Q,$$

with $R_0 := \mid \mathbf{x} - \mathbf{x_c} \mid$ being the distance from the function control point $\mathbf{x}_c$ to the point $\mathbf{x}$. The constants R_c and C control the shape of the exponential function G_q. The number of enrichment functions used is Q and the functions G_q, with $q = 1, 2, \ldots, 8$, are depicted and compared in Figure 1. It should be mentioned that a similar function to G_q was used in [32] as a weight function in the context of meshless methods when solving the linear Poisson equation. From the above, the nodal values might be rewritten as

$$C_j^n = \sum_{q=1}^{Q} A_j^{q,n} G_q. \tag{13}$$

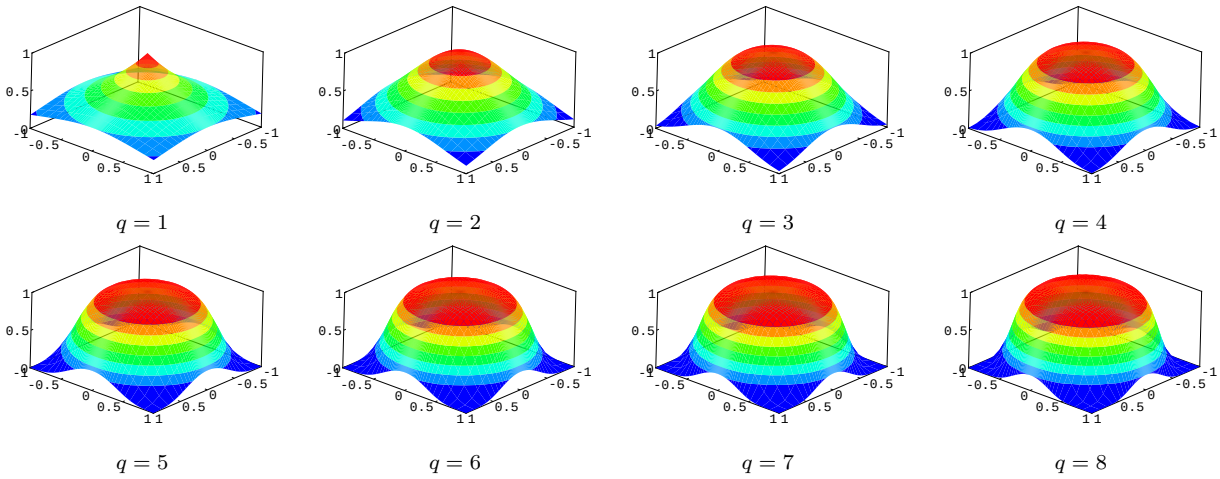

Figure 1: Illustration of the enrichment functions G_q for different values of q.

The finite element method is now used to find the values of the new set of unknowns $A_j^{q,n}$ instead of the nodal values C_j^n as before. Using (13) to rewrite (11) we obtain

$$u^n = \sum_{j=1}^{M} \sum_{q=1}^{Q} A_j^{q,n} N_j G_q. \tag{14}$$

For simplicity the multiplication of F_{enr} with the polynomial shape function is considered to be the new shape function $L_{(j-1)Q+q}$ defined by

$$L_{(j-1)Q+q} = N_j G_q. \tag{15}$$

The new approximation space then becomes

$$\widetilde{V}_h^1 = \text{span}\left\{ L_h, \qquad u_h = \sum_{j=1}^{M} \sum_{q=1}^{Q} A_j^{q,n} N_j G_q \right\}.$$

The derivatives of the new shape function are then given by

$$\frac{\partial L_{(j-1)Q+q}}{\partial x} = G_q \frac{\partial N_j}{\partial x} - q \frac{\exp\left(-\left(\dfrac{R_0}{C}\right)^q\right)}{1 - \exp\left(-\left(\dfrac{R_c}{C}\right)^q\right)} \frac{R_0^{(q-2)}}{C^q} N_j (x - x_0),$$

$$\frac{\partial L_{(j-1)Q+q}}{\partial y} = G_q \frac{\partial N_j}{\partial y} - q \frac{\exp\left(-\left(\dfrac{R_0}{C}\right)^q\right)}{1 - \exp\left(-\left(\dfrac{R_c}{C}\right)^q\right)} \frac{R_0^{(q-2)}}{C^q} N_j (y - y_0).$$

It is worth remarking that the enrichment functions F_{enr} are written in terms of the global coordinates $\mathbf{x}$, but they are multiplied by the nodal shape functions N_j. In this sense the additional enrichment takes on a local character. The change in the form of the approximation from (11) to (14) is only made locally in the vicinity of a feature of interest, such as source or sink zones.

4 Numerical Results

In this section we examine the accuracy and performance of the proposed PUFEM using three test examples. The first example solves a transient diffusion problem given by the equations (1)-(3) with an analytical solution that can be used to quantify errors in the PUFEM. The second and third examples consider the problem of heat transfer with single and multiple sources, respectively. These last examples are used to show the ability of the developed PUFEM to deal with more complicated transient diffusion problems. In what follows, we shall use the terminology FEM, PUFEM, PUFEM4DoFs, PUFEM6DoFs and PUFEM8DoFs to refer to the standard finite element method, the partition of unity finite element method, PUFEM with the number of enrichment functions $Q = 4$, 6 and 8, respectively. All the computations are made on an Intel® Xeon® PC with 24 GB of RAM and 2.93 GHz. The codes only take the default optimization of the machine, *i.e.* they are not parallel codes.

4.1 Accuracy test problem

As a first test example we consider a diffusion problem with an exact solution in a square domain $\Omega = [0, 2] \times [0, 2]$. We solve the transient equation (1)-(3) with the reaction term f, the boundary function g and the initial condition u_0 are being explicitly calculated such that the exact solution of the problem (1)-(3) is given by

$$U(x, y, t) = x^{20} y^{20} (2 - x)^{20} (2 - y)^{20} \Big(1 - \exp(-\lambda t)\Big), \tag{16}$$

Note that in order to avoid having the exact solution (16) as a subset of the enrichment space, it is manufactured using high order polynomials rather than exponential functions in the space domain. To quantify the errors in this test example we consider the L^2-norm error defined as

$$\varepsilon_2 = \frac{\|u - U\|_{L^2(\Omega)}}{\|U\|_{L^2(\Omega)}}, \tag{17}$$

where $\|\cdot\|_{L^2(\Omega)}$ is the L^2 norm, u and U are respectively, the computed and exact solutions. In all presented computations the parameter $\alpha = 1$, the time step $\Delta t = 0.1$

4.1.1 Integration points

	h_1			$h_{\frac{1}{2}}$		
Δt	4DoFs	6DoFs	8DoFs	4DoFs	6DoFs	8DoFs
0.5	0.067	0.069	0.064	0.0172	0.0114	0.0106
0.1	0.064	0.065	0.061	0.0127	0.0042	0.0029
0.01	0.064	0.066	0.061	0.0121	0.0033	0.0018

Table 1: L^2-norm error for a decreased time step Δt for the PUFEM with different enrichment numbers and mesh grids when $\lambda = 0.1$ is considered at $t = 1s$.

4.1.2 Time step

4.1.3 Convergence study

and the diffusion coefficient λ is selected to take the values 0.1 and 0.01. The aim of this test example is to compare the results obtained using the proposed PUFEM to those obtained using

	h_1			$h_{\frac{1}{2}}$		
Δt	4DoFs	6DoFs	8DoFs	4DoFs	6DoFs	8DoFs
0.5	8.87	14.32	16.83	10.64	17.32	18.53
0.1	9.40	14.86	18.07	10.73	16.65	17.14
0.01	10.15	15.68	17.23	11.49	16.96	17.65

Table 2: Condition number $\log(\kappa)$ for a decreased time step Δt for the PUFEM with different enrichment numbers and mesh grids when $\lambda = 0.1$ is considered at $t = 1s$.

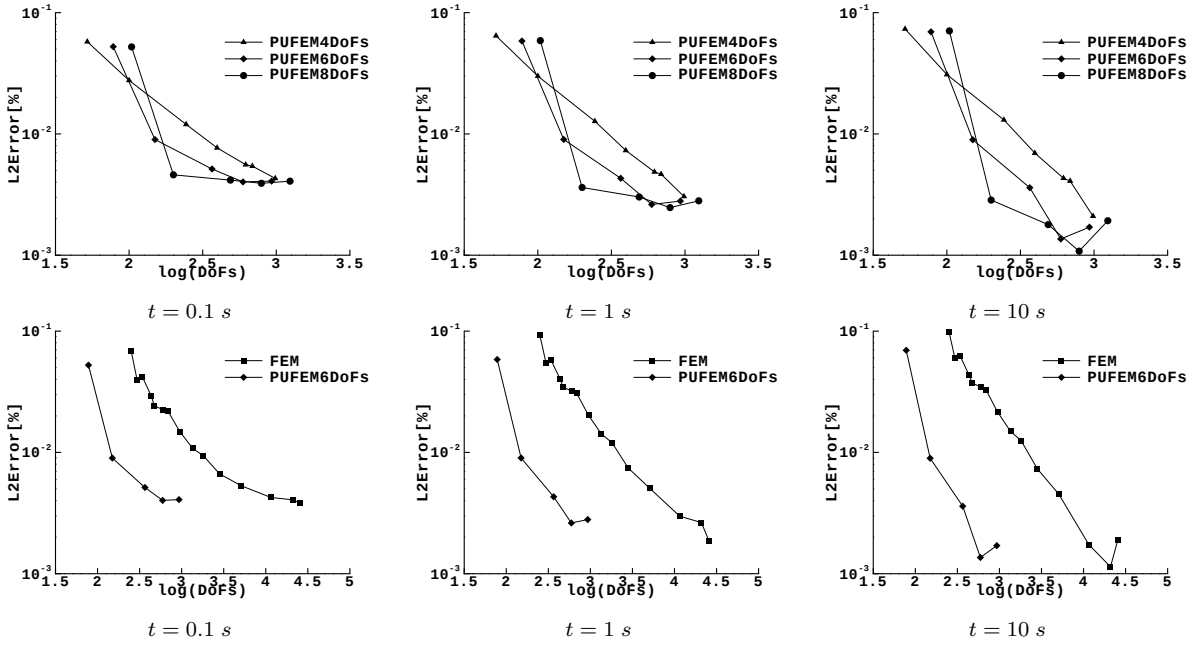

Figure 2: Convergence history of the measured relative error ε_2 for the accuracy test problem at different simulation times using $\lambda = 0.1$. On the bottom are the comparative results between FEM and PUFEM methods.

the standard FEM. To this end we consider three numbers of enrichment functions; $Q = 4$, 6 and 8. To study the convergence of the FEM, PUFEM4DoFs, PUFEM6DoFs and PUFEM8DoFs each of them is considered with further h-refinements. To evaluate elementary matrix entries all the integrals are evaluated numerically using Gaussian quadrature. The resulting linear system is solved using a direct solver. Figure 2 and Figure 3 show, respectively, the convergence and the conditioning of the proposed methods for an increasing number of Degrees of Freedom (DoFs) when $\lambda = 0.1$. The top three plots of Figure 2 compare the convergence of the PUFEM for an increased number Q of enrichment functions while the bottom figures compare the convergence of the PUFEM6DoFs to that of the FEM. The numerical results correspond to the simulation times $t = 0.1$,1 and 10. A similar set of results for $\lambda = 0.01$ are shown in Figure 4 and Figure 5.

In the above set of results and for both values of λ, it is clear that the PUFEM converges much faster compared to the FEM. To achieve an error $\varepsilon_2 = 0.004$ and for $\lambda = 0.1$, 11542 degrees of freedom are needed with the FEM whereas with the PUFEM6DoFs this is reduced to 930. To build the FEM linear system at the first time step, in this case, 2.43 s of CPU time are needed and another 177.54 s to solve it. The corresponding times with the PUFEM6DoFs are 0.56 s and 0.06 s, respectively. With the PUFEM6DoFs, 21 integration points are needed while with the FEM 3 points are enough; yet the much larger number of elements with the FEM (22686 elements)

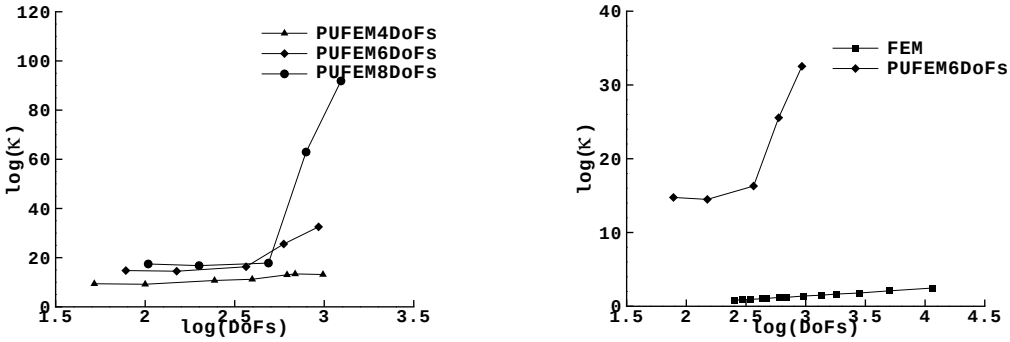

Figure 3: Condition number plotted with respect to the number of degrees of freedom for the accuracy test problem at time $t = 1$ using $\lambda = 0.1$. On the right are the comparative results between FEM and PUFEM methods.

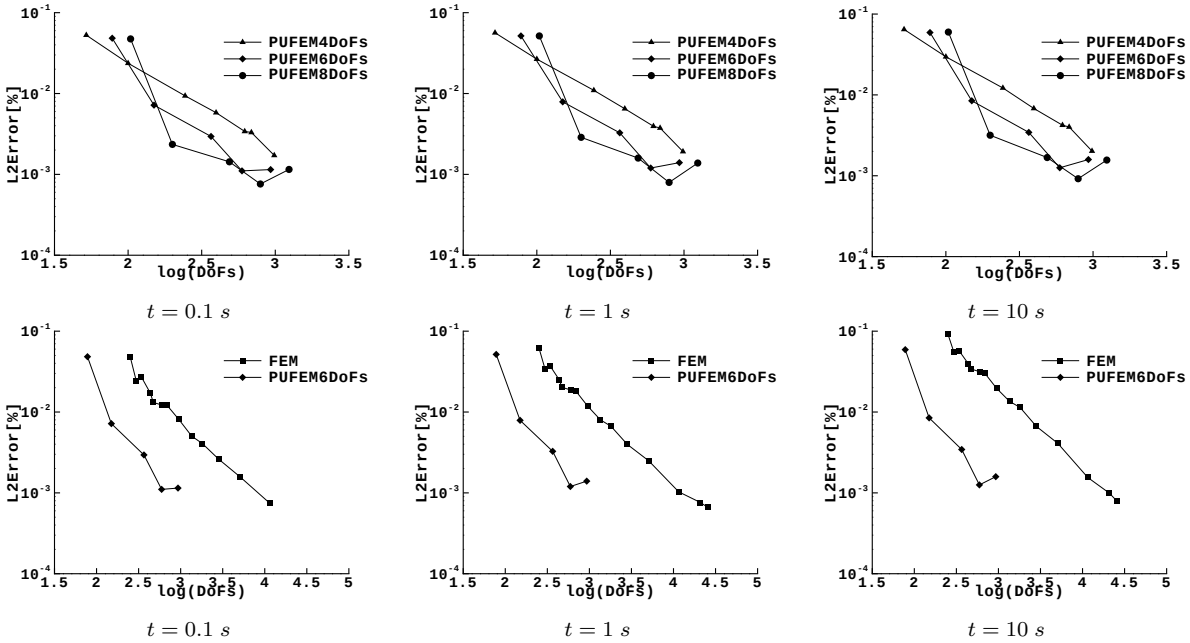

Figure 4: The same as Figure 2 but using $\lambda = 0.01$.

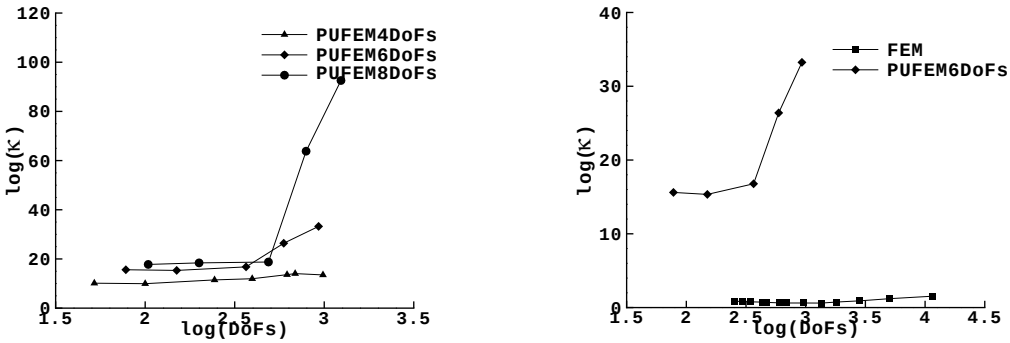

Figure 5: The same as Figure 3 but using $\lambda = 0.01$.

makes the time needed to build the system matrix more than that with the PUFEM6DoFs (264 elements). Because the PUFEM6DoFs linear system is much smaller compared to the FEM, the CPU time for solving the PUFEM6DoFs system is only a small fraction of that of the FEM. It should be noted that the relatively long time needed to build the PUFEM6DoFs system matrix compared to solving it, is caused by the time spent on evaluating the enrichment functions and the higher number of integration points used. However, the system matrix is only evaluated at the first time step. Compared to the finite element case where the system matrix can be decomposed and reused at later time steps as well as in the present approach, other enrichment methods with repeatedly evaluating and solving the linear system, may have a major disadvantage.

In general as a higher number of enrichment functions is considered the same error seems to be achievable using a lower number of degrees of freedom. However, the conditioning seems to affect the accuracy of the PUFEM. Figure 3 and Figure 5 show much higher condition numbers for the PUFEM compared to the FEM. The conditioning degrades very quickly as a higher number of enrichment functions is considered. This may be anticipated as the enrichment functions start with relatively sharp gradients closer to the source and then rapidly flatten out at higher orders. The difference between two enrichment functions becomes smaller as higher orders are considered. After a certain value of Q the difference gets beyond the machine precision, resulting in a singular system. To avoid this limitation, values of Q up to 8 are considered in this subsection while in subsections 4.2 and 4.3 only $Q = 6$ is used. It should be mentioned here that double precision variables and a direct solver are used to deal with the high conditioning. However, a direct solver is needed to decompose the system matrix at the first time step in order to make use of it at subsequent time steps by just updating the right hand side and using a backward/forward substitution to solve the next linear systems. Otherwise with an iterative solver the linear system has to be resolved at every time step.

The results with the PUFEM or the FEM do not seem to be changing significantly with time. This is particularly true for $\lambda = 0.01$ and can be explained by the nature of the exact solution where the source flattens out slowly with time. However, for $\lambda = 0.1$ the source flattens out faster than the previous case resulting in less sharp gradients at later time steps which can be captured easier with the FEM and the PUFEM.

4.2 Single heat source

This example solves a diffusion problem governed by the equations (1)-(3) in a circular domain of radius $r = 1\ m$ and a rectangular heat source located in the center of the computational domain as illustrated in Figure 6. The thermal conductivity of the medium is assumed to be $\lambda = 0.01\ kg\ m/K\ s^2$ and the convective heat transfer coefficient $\alpha = 1\ kg/K\ s^2$. We consider an instantaneous heat source given by

$$f(t,x,y) = \begin{cases} 1800\ K/s, & \text{if} \quad (x,y) \in [0.8,0.9] \times [1.2,1.1] \qquad \text{and} \qquad t \leq 5\ s, \\ \\ 300\ K/s, & \text{elsewhere.} \end{cases}$$

Initially the medium is set at the temperature $u_0 = 300\ K$ and the boundary temperature $g = 300\ K$. The time step is fixed to $\Delta t = 0.5\ s$. The numerical results are presented at three different times $t = 0.5, 5$ and $10\ s$.

The purpose of this test example is to compare the PUFEM to the standard FEM using different meshes. Here we consider three unstructured meshes with different element densities as depicted in Figure 7. The fine mesh (FEM1) is used with the FEM to compute a reference solution for the considered test example. The other two meshes (PUFEM6Dof and FEM2) are used to compare the PUFEM results against the FEM where a comparable number of DoFs is used that is 822 for the PUFEM6DoFs and 1437 for the FEM1. All the integrals are evaluated using Gaussian quadrature with 3 points for the FEM and 36 points for the PUFEM6DoFs.

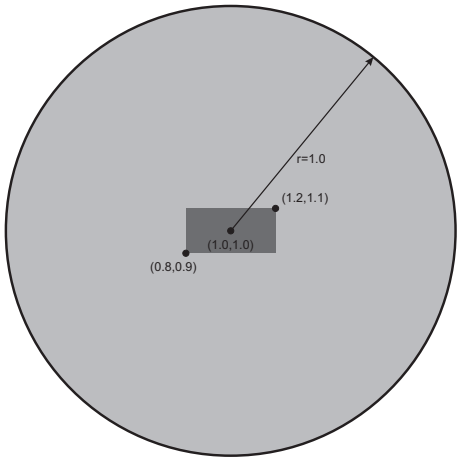

Figure 6: Configuration for the test example of the single heat source problem. The numbers refer to the coordinates in meters.

In Figure 8 we display the temperature distributions obtained using the PUFEM6DoFs against the reference solution at the times $t = 0.5$, 5 and 10 s which are: shortly after the source application started, the source application ended and 5 seconds after the source application ended, respectively. The results obtained with the PUFEM6DoFs show the same temperature trends as those obtained using the FEM1. It is evident that for the considered thermal conditions, both the FEM1 and the PUFEM6DoFs capture the solution dynamics and accurately resolve the moving temperature fronts. However, the FEM1 results are obtained on a fine mesh with 17720 elements and 9017 nodes while, the PUFEM results are computed using a coarse mesh with 240 elements and 137 nodes and 6 enrichment functions which is a significant reduction of the total number of degrees of freedom. As can be seen from this figure, the temperature starts to increase due to the heat source included in the center of the domain then the source ceases and the medium starts to cool down. For both methods, the temperature field in this figure shows the simulated moving fronts from the source location towards the walls at the surrounding temperature.

In order to illustrate the effectiveness of the proposed PUFEM, we compare in Figure 9 the cross sections of the difference between the FEM2 and the reference solution (top three figures) and the PUFEM6DoFs and the reference solution (bottom three figures) along the horizontal center line for the three selected times. The cross sections along the vertical center line are illustrated in Figure 10. These differences are used to express the error rather than using the L2Error as in the previous case because the local differences in the source vicinity may have a crucial effect on the physical properties of the considered material locally even though the L2error may still seem within acceptable limits.

The PUFEM6DoFs and the FEM2 results show two different behaviors during and after the source application. The local errors at the stage of heat release are larger with the FEM2 compared to the PUFEM6DoFs. This is attributed to the high temperature gradient at this stage which is better captured using the enrichment functions. However, at the cooling stage when heat starts to diffuse through the boundary, the computed differences for both methods are of similar magnitude. The differences with the PUFEM6DoFs appear relatively large at the boundary rather than the central domain. This can be improved through better geometrical representation of the boundary by using for example higher order elements instead of the linear elements used in current study. However, at this stage the heat becomes more uniformly distributed. This relatively flat distribution is easier to capture with the FEM even when a coarse mesh is used. It should be added that for general engineering applications the stage with high heat gradients is usually the most crucial.

To further quantify the results for this test example we plot in Figure 11 the time evolution

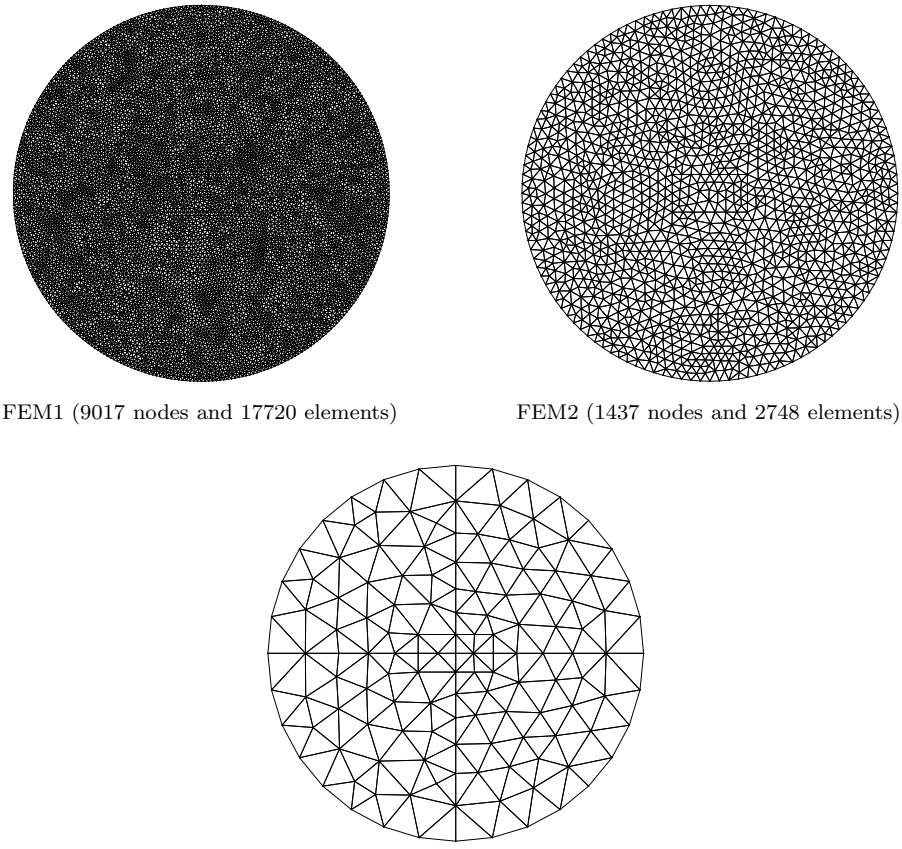

Figure 7: Finite element meshes for the test example of the single heat source problem.

of the maximum temperature differences in the medium, obtained using the PUFEM6DoFs and FEM2 (the horizontal center line is plotted to the left while the vertical is to the right). The behavior described above becomes even more evident. After the heat source is switched off both the PUFEM6DoFs and the FEM2 results decay to a steady state difference. The CPU times to build the linear systems of the FEM1, FEM2 and PUFEM6DoFs are 1.76, 0.56 and 0.46 s, respectively. The associated CPU times to solve these systems, in the same order, are: 90.62, 0.25, 0.03 s. These values are given for the first time step but in subsequent steps these linear systems are retained. The results show a significant saving in the computation time when the PUFEM6DoFs is used compared to the FEM1. The PUFEM6DoFs leads to better results compared to the FEM2 even though a smaller number of DoFs is used and with a significant reduction of the solution cost. This is true despite the fact that the enrichment functions are axisymmetric while the selected heat source is not; the approximation can be improved by considering an enrichment that is more elongated in the horizontal direction than in the vertical. However, in this study we choose to select a more general form of enrichment.

4.3 Multiple heat sources

Our final test example consists of solving a problem with multiple heat sources. The governing equations are given in expressions (1)-(3) and the thermal characteristics of the medium are the same as in the previous problem with a single heat source. The dimensions of the computational

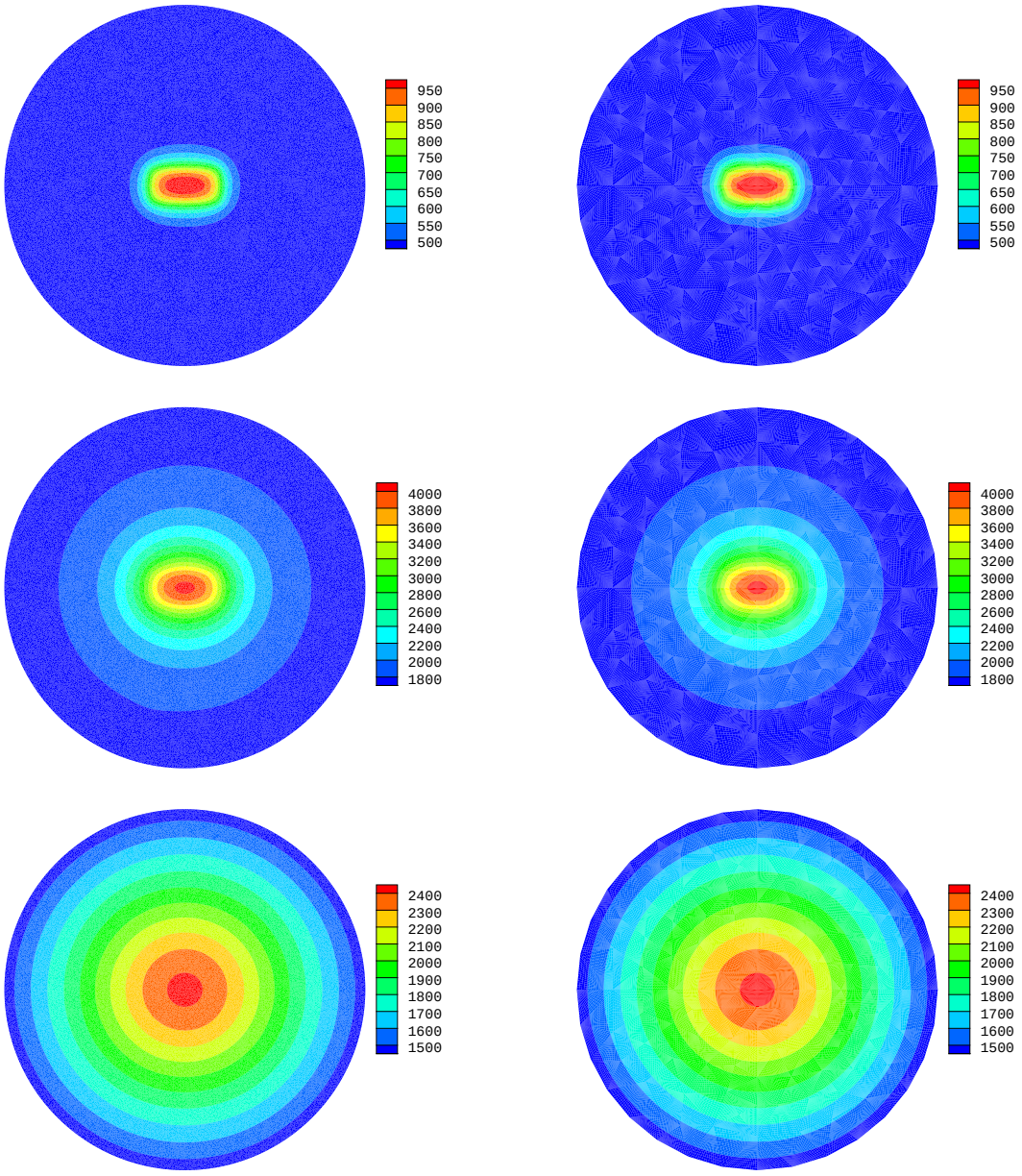

Figure 8: Temperature distributions obtained using the FEM1 (left) and PUFEM6DoFs (right) for the test example of the single heat source problem. From top to bottom the simulation time $t = 0.5$, 5 and 10 s.

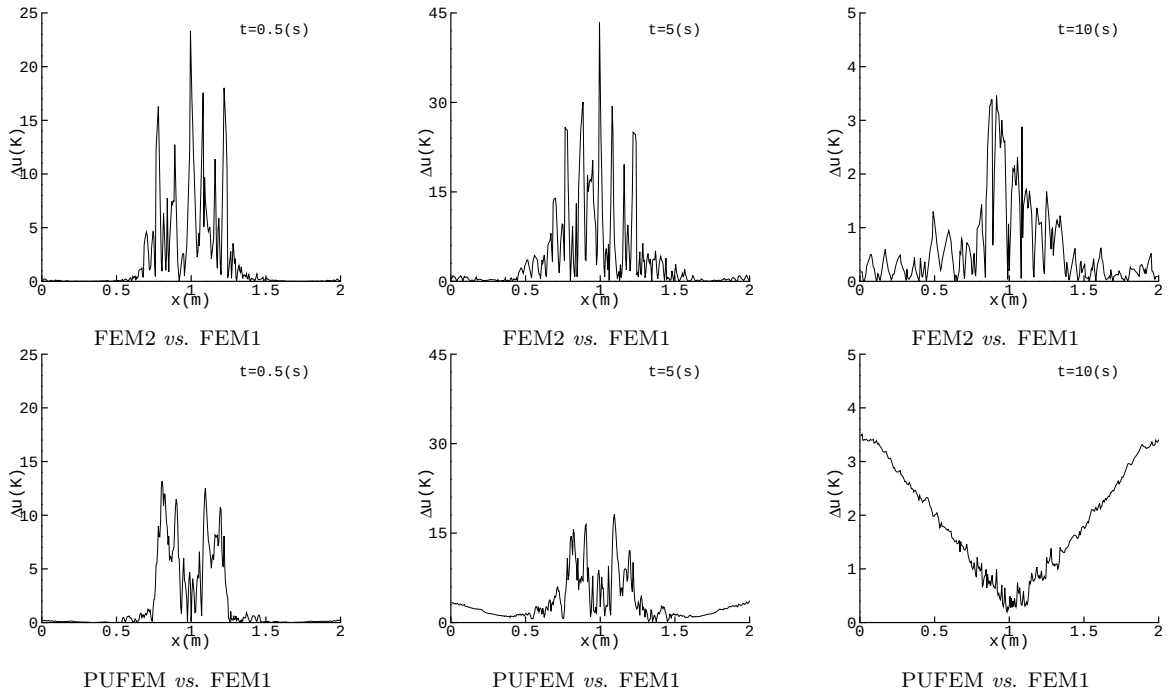

Figure 9: Variation of the temperature differences between the FEM1 and the reference solutions (top), PUFEM6DoFs and the reference solutions (bottom) along the horizontal direction for the test example of the single heat source problem.

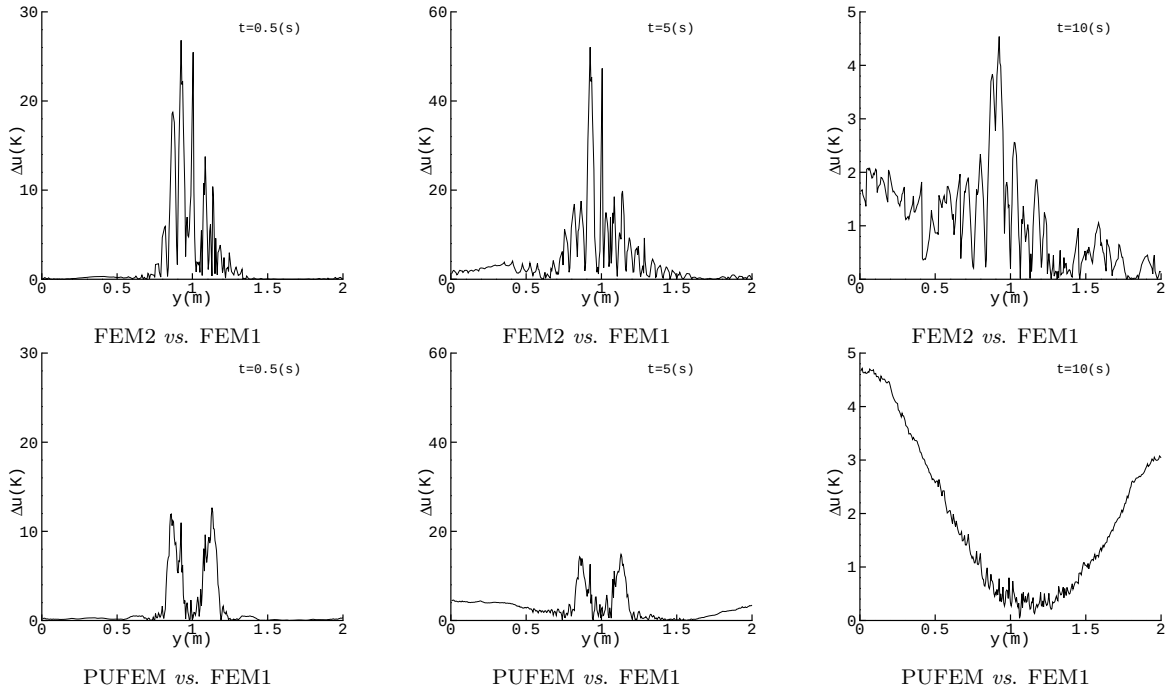

Figure 10: Variation of the temperature differences between the FEM1 and the reference solutions (top), PUFEM6DoFs and the reference solutions (bottom) along the vertical direction for the test example of the single heat source problem.

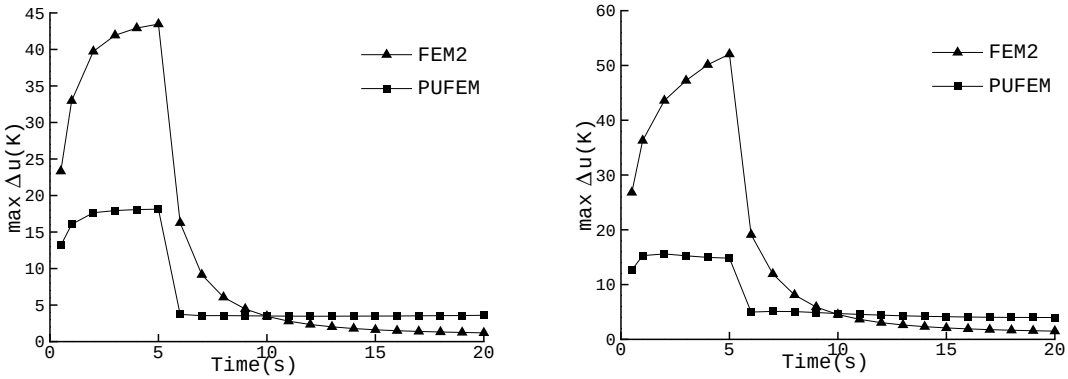

x-direction y-direction

Figure 11: Time evolution of variation of the temperature differences along the horizontal direction (left) and along the vertical direction (right) for the test example of the single heat source problem.

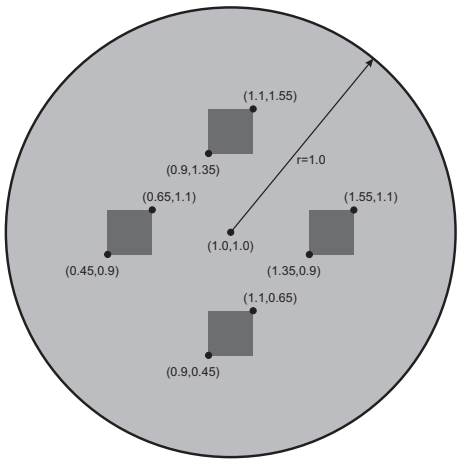

Figure 12: Configuration for the test example of the multiple heat sources problem. The numbers refer to the coordinates in meters.

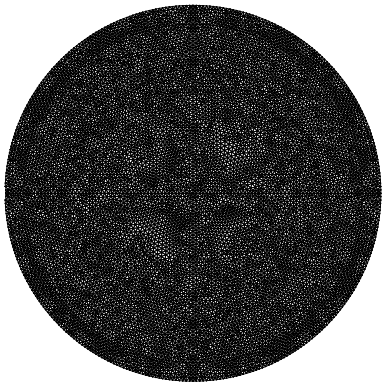

FEM1 (11041 nodes and 21732 elements)

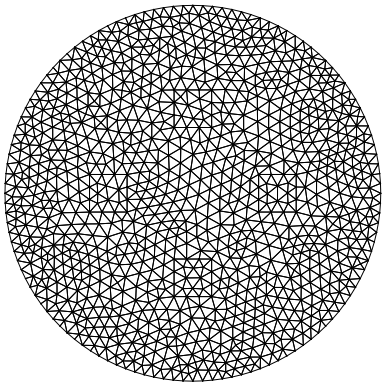

FEM2 (1076 nodes and 2030 elements)

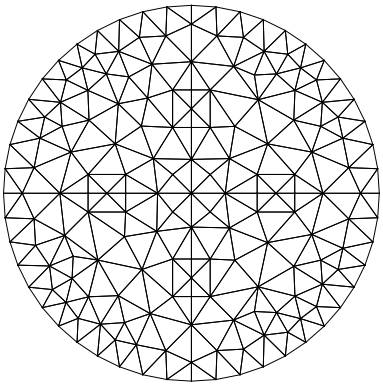

PUFEM6DoFs (178 nodes and 306 elements)

Figure 13: Finite element meshes for the test example of the multiple heat sources problem.

domain are shown in Figure 12 with four embedded heat sources defined as

$$f(t,x,y) = \begin{cases} 1300\ K/s, & \text{if} \quad (x,y) \in [0.45, 0.90] \times [0.65, 1.10] \quad \text{and} \quad t \leq 5\ s, \\ 1800\ K/s, & \text{if} \quad (x,y) \in [1.35, 0.90] \times [1.55, 1.10] \quad \text{and} \quad t \leq 5\ s, \\ 2300\ K/s, & \text{if} \quad (x,y) \in [0.90, 0.45] \times [1.10, 0.65] \quad \text{and} \quad t \leq 5\ s, \\ 2800\ K/s, & \text{if} \quad (x,y) \in [0.90, 1.35] \times [1.10, 1.55] \quad \text{and} \quad t \leq 5\ s, \\ 300\ K/s, & \text{elsewhere.} \end{cases}$$

In contrast to the previous test example, multiple sources with different heat capacity are embedded in the domain. As a consequence, the symmetry is not preserved in the temperature field and this thermal problem is relatively more difficult to handle. Furthermore, the considered heat problem is an unsteady problem in nature; therefore, good numerical accuracy is required in order to capture the different phenomena present in its evolving solution.

The comparison study of this test example is designed similarly to the previous one where three meshes are used with the reference solution based on the finest mesh and the FEM solution. Figure 13 presents the three meshes considered in the simulations. In this example the number of degrees of freedom in the reference solution is 11041. A much lower number is used with the PUFEM6DoFs and the FEM2 that is 1068 and 1076, respectively. The time step is again taken $\Delta t = 0.5\ s$. To handle multiple sources in this example each enrichment function is taken to be the sum of four functions G_q that are of the same order q but centered at a different source. All the integrals are evaluated using Gaussian quadrature with 3 points for the FEM1 and FEM2 and 36 points for the PUFEM6DoFs. A direct solver is also used for the resulting linear systems.

In Figure 14 we show snapshots of the temperature using the FEM1 and PUFEM6DoFs results at the considered times. As expected, for the different values of the temperature at the sources the thermal fronts travel faster towards the domain center. The results obtained with the PUFEM6DoFs show close similarities to those of the reference solutions. Again FEM2 and PUFEM6DoFs are compared to the reference solution by computing the differences along the horizontal and vertical center lines which are presented in Figure 15 and Figure 16, respectively. As in the previous test example, the errors at the release stage of the heat are larger than those calculated at the cooling stage as the high temperature gradients start to decrease. From these figures one can observe that the PUFEM6DoFs errors are smaller than the FEM2 errors at the release stage but not at the cooling stage. Again here similar remarks may be made as in the previous case. The proposed PUFEM performs very satisfactorily for this heat problem since it does not diffuse the moving fronts and no spurious oscillations have been detected near steep gradients of the temperature field in the computational domain. The results obtained using PUFEM are the most accurate compared to those of the FEM2 where a similar number of degrees of freedom is used. For visualizing the comparisons, we display in Figure 17 the time evolution of the maximum temperature differences in the medium obtained using the PUFEM6DoFs and FEM2. Under the thermal conditions, it is clear that the cross section plots exhibited different behaviors before and after the heat sources are switched off. To have an insight into the computational costs of this test example the CPU time is compared for the three considered solutions. To build the linear systems with the FEM1, FEM2 and PUFEM6DoFs the CPU times are 2.21, 0.51 and 0.68 s, respectively. The corresponding times needed to solve these systems are 20.73, 0.1 and 0.06 s, respectively. This suggests a significant saving in the computations time when the PUFEM6DoFs is used. The time comparison shows that building the linear system with the PUFEM6DoFs becomes more expensive compared to FEM2. That is due to the time needed to evaluate a relatively large number of functions besides the relatively large number of integration points. However, this computational cost may still be justifiable given the accuracy improvement at the heat release stage and given

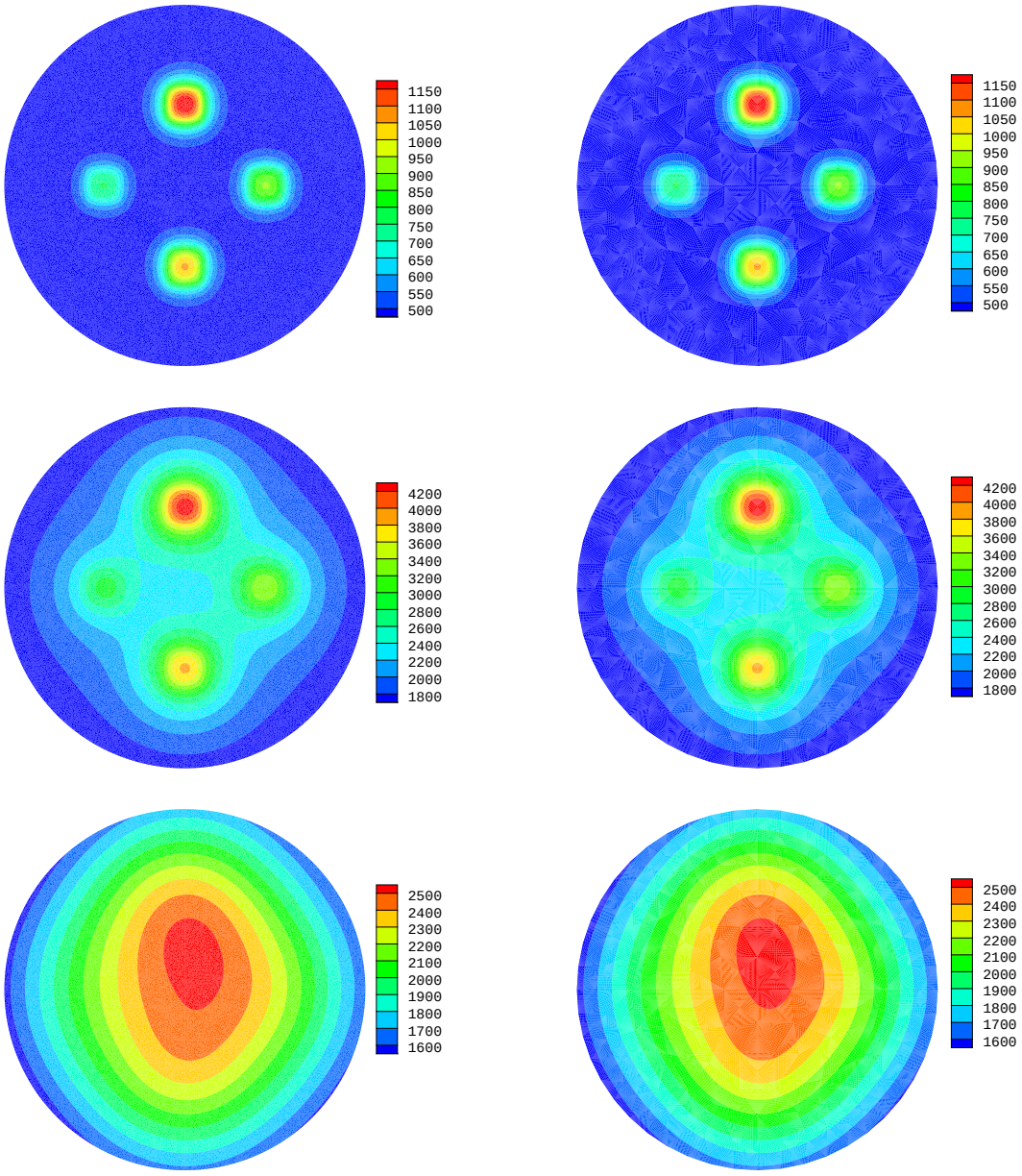

Figure 14: Temperature distributions obtained using the FEM1 (left) and PUFEM6DoFs (right) for the test example of the multiple heat sources problem. From top to bottom the simulation time $t = 0.5$, 5 and 10 s.

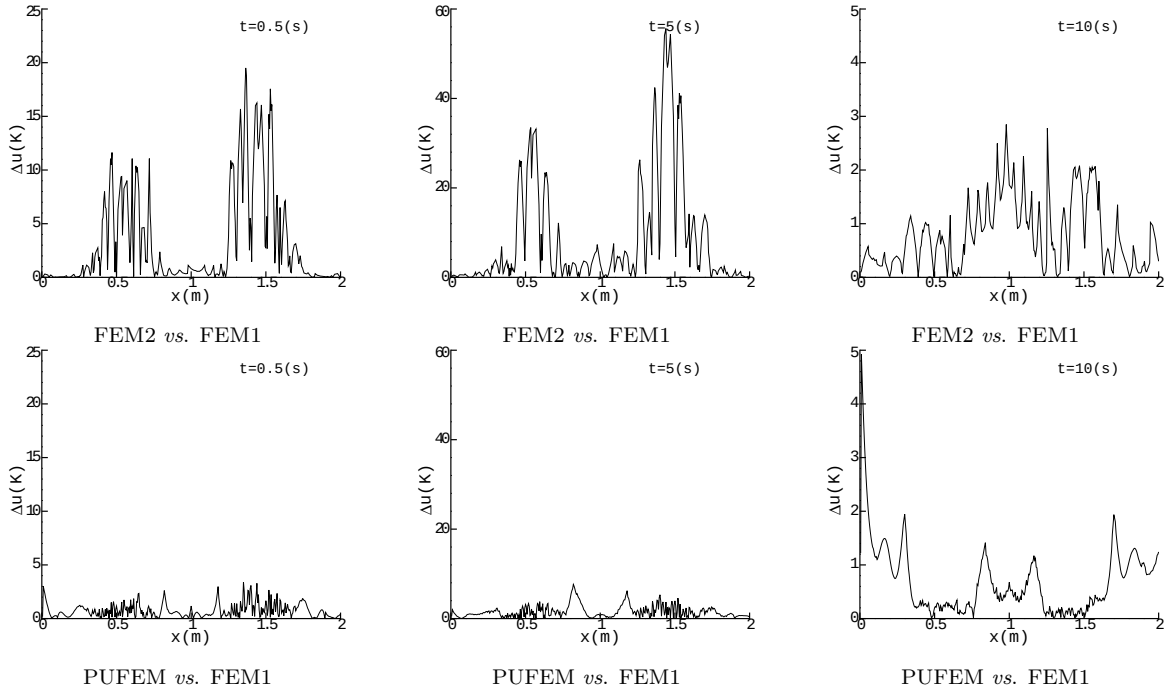

Figure 15: Variation of the temperature differences between the FEM2 and the reference solutions (top), PUFEM6DoFs and the reference solutions (bottom) along the horizontal direction for the test example of the multiple heat sources problem.

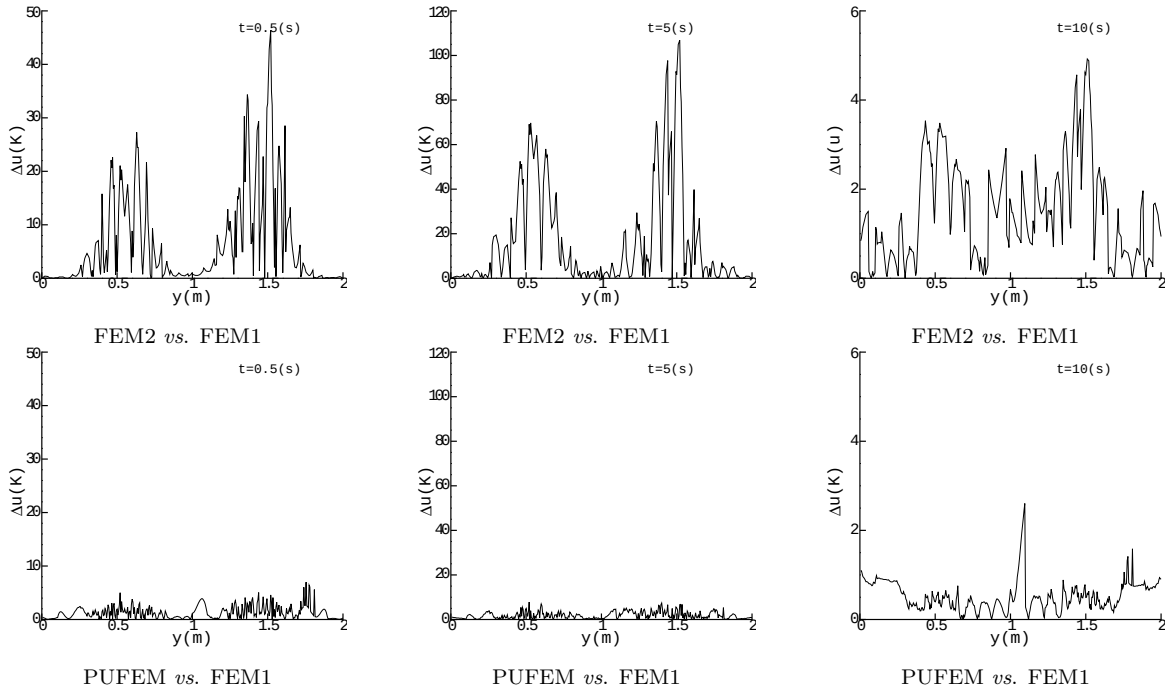

Figure 16: Variation of the temperature differences between the FEM2 and the reference solutions (top), PUFEM6DoFs and the reference solutions (bottom) along the vertical direction for the test example of the multiple heat sources problem.

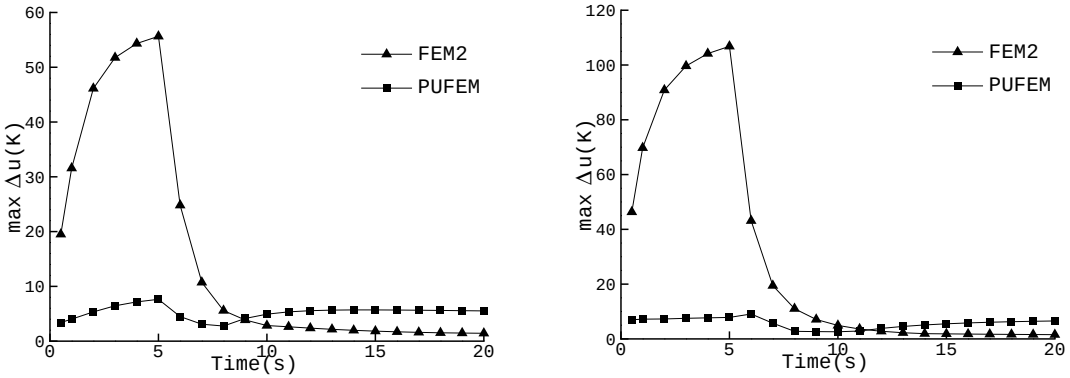

x-direction y-direction

Figure 17: Time evolution of variation of the temperature differences along the horizontal direction (left) and along the vertical direction (right) for the test example of the multiple heat sources problem.

that the linear system is only assembled once. It is even possible to significantly reduce the time needed to build the PUFEM linear system if an analytical integration scheme is to be used.

5 Conclusions

An enriched partition of unity finite element method is proposed to solve time dependent diffusion problems. An approximate solution describing the diffusion decay is embedded in the finite element shape functions. The enrichment used to construct the approximation is exponential and mimics the spatial and temporal behavior of the solution. These approximation properties can lead to a significant saving in the computational costs compared to only spatial approximation enrichments that change at each time step. Especially that the time needed to build the linear system is increased significantly due to the relatively high number of integration points may be needed to integrate the enrichment functions. Hence, assembling the system matrix only once can significantly improve the efficiency compared to evaluating the system matrix at each time step. The system matrix can be decomposed at the first time step and then reused after updating the right hand side to solve the linear system at the following time steps. The advantage of this method compared to *hp*-FEM is its ability to locally refine the solution by adapting the enrichment instead of creating a new mesh. The favorable performance of the developed partition of unity finite element method has been demonstrated using a series of numerical examples, including the non-stationary heat equation with multiple sources. Numerical comparisons have been carried out for all the considered methods, FEM and PUFEM, in terms of accuracy and efficiency. It is shown that for a fixed accuracy the total number of degrees of freedom may be reduced by up to 90% when the PUFEM is used. The conditioning issue, which may affect the use of iterative solvers with the proposed method, is discussed. However, a direct solver is needed to decompose the system matrix otherwise the system has to be resolved at every time step if an iterative solver is to be used.

In general, the partition of unity finite element method shows higher accuracy than the conventional finite element method for a fixed number of degrees of freedom. The results obtained show that the partition of unity finite element method has the advantage of requiring less computational resources for the time dependent diffusion problems than a conventional finite element method, typical of those widely used in the finite element solution of elliptic PDEs. This fact, as well as its favorable stability properties, make it an attractive alternative for diffusion solvers based on finite element techniques.

Although we have restricted our numerical computations to the case of two-dimensional tran-

sient diffusion problems using linear finite elements, the more important implications of our research concern the use of the effective enriched partition of unity method for computational heat transfer problems in three spatial dimensions implemented in parallel processing. Our current effort is therefore to extend these methods for the coupled conduction radiation problems in higher space dimensions using unstructured meshes. Future work will also concentrate on developing efficient adaptive enrichment for transient diffusion problems in heterogeneous media with discontinuous coefficients. The algorithms presented in this paper can be highly optimized for the vector computers, because they do not require nonlinear solvers and contain no recursive elements. Some difficulties arise from the fact that for efficient vectorization the data should be stored continuously within long vectors rather than two-dimensional arrays.

References

[1] M. Seaïd. An eulerian-lagrangian method for coupled parabolic-hyperbolic equations. *Appl. Numer. Math.*, 59:754–768, 2009.

[2] A. Klar, J. Lang, and M. Seaïd. Adaptive solutions of SP_N-approximations to radiative heat transfer in glass. *Int. J. Therm. Sci.*, 44:1013–1023, 2005.

[3] M. Seaïd. Multigrid newton-krylov method for radiation in diffusive semitransparent media. *J. Comp. Applied Math.*, 203:498–515, 2007.

[4] R. Viskanta and E.E. Anderson. Heat transfer in semitransparent solids. *Adv. Heat Transfer*, 11:318–441, 1975.

[5] G. Thömmes, R. Pinnau, M. Seaïd, and A. Klar Th. Götz. Numerical methods and optimal control for glass cooling processes. *Transp. Theory Stat. Phys.*, 31:513–529, 2002.

[6] M. Frank, A. Klar, E.W. Larsen, and S. Yasuda. Time-dependent simplified pn approximation to the equations of radiative transfer. *J. Comput. Phys.*, 226:2289–2305, 2007.

[7] A.D. Klose and E.W. Larsen. Light transport in biological tissue based on the simplified spherical harmonics equations. *J. Comput. Phys.*, 220:441–470, 2006.

[8] J.M. Melenk and I. Babuška. The partition of unity finite element method: Basic theory and applications. *Comput. Methods Appl. Mech. Engrg*, 139:289–314, 1996.

[9] N. Moës, J. Dolbow, and T. Belytschko. A finite element method for crack growth without remeshing. *Int. J. Numer. Meth. Engng.*, 46:131–150, 1999.

[10] V.P. Nguyen, T. Rabczuk, S. Bordas, and M. Duflot. Meshless methods: a review and computer implementation aspects. *Math. Comput. Simul.*, 79:763–813, 2008.

[11] R. Simpson and J. Trevelyan. A partition of unity enriched dual boundary element method for accurate computations in fracture mechanics. *Comput. Methods Appl. Mech. Engrg.*, 200:1–10, 2011.

[12] O. Laghrouche, P. Bettess, E. Perrey-Debain, and J. Trevelyan. Wave interpolation finite elements for Helmholtz problems with jumps in the wave speed. *Comput. Methods Appl. Mech. Engrg.*, 194:367–381, 2004.

[13] A. El-Kacimi and O. Laghrouche. Numerical modelling of elastic wave scattering in frequency domain by the partition of unity finite element method. *Int. J. Numer. Meth. Engng.*, 77:1646–1669, 2009.

[14] O. Laghrouche and M.S. Mohamed. Locally enriched finite elements for the Helmholtz equation in two dimensions. *Comput. Struct.*, 88:1469–1473, 2010.

[15] E. Perrey-Debain, J. Trevelyan, and P. Bettess. Wave boundary elements: a theoretical overview presenting applications in scattering of short waves. *Eng. Anal. Bound. Elem.*, 28:131–141, 2004.

[16] S. Langdon and S.N. Chandler-Wilde. A wavenumber independent boundary element method for an acoustic scattering problem. *SIAM J. Numer. Anal.*, 43:2450–2477, 2006.

[17] O. Cessenat and B. Despres. Application of the ultra-weak variational formulation of elliptic pde's to the two-dimensional Helmholtz problem. *SIAM J. Numer. Anal.*, 35:255–299, 1998.

[18] T. Huttunen, P. Monk, F. Collino, and J.P. Kaipio. The ultra weak variational formulation for elastic wave problems. *SIAM J. Sci. Comp.*, 25:1717–1742, 2004.

[19] T. Huttunen, P. Gamallo, and R.J. Astley. Comparison of two wave element methods for the Helmholtz problem. *Commun. Numer. Meth. En.*, 25:35–52, 2009.

[20] R. Tezaur, L. Zhang, and C. Farhat. A discontinuous enrichment method for capturing evanescent waves in multiscale fluid and fluid/solid problems. *Comput. Methods Appl. Mech. Engrg.*, 197:1680–1698, 2008.

[21] R. Tezaur and C. Farhat. Three-dimensional discontinuous Galerkin elements with plane waves and Lagrange multipliers for the solution of mid-frequency Helmholtz problems. *Int. J. Numer. Meth. Eng.*, 66:796–815, 2006.

[22] L. Zhang, R. Tezaur, and C. Farhat. The discontinuous enrichment method for elastic wave propagation in the medium-frequency regime. *Int. J. Numer. Meth. Eng.*, 66:2086–2114, 2006.

[23] C.A. Duarte and D.J. Kim. Analysis and applications of a generalized finite element method with global-local enrichment functions. *Comput. Methods Appl. Mech. Engrg.*, 197:487–504, 2008.

[24] T. Strouboulis, I. Babuška, and R. Hidajat. The generalized finite element method for Helmholtz equation: Theory, computation, and open problems. *Comput. Methods Appl. Mech. Engrg.*, 195:4711–4731, 2006.

[25] T. Strouboulis, R. Hidajat, and I. Babuška. The generalized finite element method for Helmholtz equation part II: Effect of choice of handbook functions, error due to absorbing boundary conditions and its assessment. *Comput. Methods Appl. Mech. Engrg.*, 197:364–380, 2008.

[26] H. Waisman and T. Belytschko. Parametric enrichment adaptivity by the extended finite element method. *Int. J. Numer. Meth. Engng.*, 73:1671–1692, 2008.

[27] J. Trevelyan and G. Coates. On adaptive definition of the plane wave basis for wave boundary elements in acoustic scattering: the 2D case. *Comput. Model. Eng. Sci.*, 55:147–170, 2010.

[28] P. O'Hara, C.A. Duarte, and T. Eason. Generalized finite element analysis of three-dimensional heat transfer problems exhibiting sharp thermal gradients. *Comput. Methods Appl. Mech. Engrg.*, 198:1857–1871, 2009.

[29] F.P. van der Meer, R. Al-Khoury, , and L.J. Sluys. Time-dependent shape functions for modeling highly transient geothermal systems. *Int. J. Numer. Meth. Engng.*, 77:240–260, 2009.

[30] P. O'Hara, C.A. Duarte, and T. Eason. Transient analysis of sharp thermal gradients using coarse finite element meshes. *Comput. Methods Appl. Mech. Engrg.*, 200:812–829, 2011.

[31] X. Li. On solving boundary value problems of modified Helmholtz equations by plane wave functions. *J. Comput. Appl. Math.*, 195:66–82, 2006.

[32] S. N. Atluri and T. Zhu. A new meshless local Petrov-Galerkin (MLPG) approach in computational mechanics. *Comput. Mech.*, 22:117–127, 1998.